Simultaneous electrochemical detection of oxygen (O2) and hydrogen peroxide (H2O2) in neutral media

Guillaume Gotti, David Evrard, Pierre Gros

International Journal of Electrochemical Science 18 (2023) 100262

Contents lists available at ScienceDirect

International Journal of Electrochemical Science

journal homepage: www.journals.elsevier.com/ijoes

Simultaneous electrochemical detection of oxygen (O_2) and hydrogen peroxide (H_2O_2) in neutral media

Guillaume Gotti, David Evrard*, Pierre Gros

Laboratoire de Génie Chimique, Université de Toulouse, CNRS, INPT, UPS, Toulouse, France

ARTICLE INFO

Keywords:
Simultaneous detection of oxygen and hydrogen peroxide
Functionalized electrode
Electrodeposited and chemically synthesized gold nanoparticles
Electrochemical kinetics study
Anodic transfer coefficient

ABSTRACT

The simultaneous detection of oxygen (O_2) and hydrogen peroxide (H_2O_2) in neutral media was investigated by cyclic voltammetry using a two-working modified glassy carbon (GC) electrode system. Both electrodes were functionalized either by electrodeposited or by chemically-prepared gold nanoparticles (AuNPs). AuNPs electrodeposition was achieved by constant potential electrolysis either at 0.5 or -0.5 V/SHE in acidic $HAuCl_4$ solution. Colloidal AuNPs were obtained according four different procedures (type A to D) derived from the classical Turkevich synthesis and further drop-casted on GC. The kinetics of H_2O_2 oxidation was studied by recording steady-state voltammograms in a deaerated $NaCl/NaHCO_3$ pH 7.4 neutral solution on all the functionalized electrodes and favorably compared to unmodified GC and bare gold electrodes. Both Koutecky-Levich and Tafel treatment of the current-potential curves showed that the highest anodic transfer coefficient α_n (0.78 ± 0.14) was obtained with the electrodeposited AuNPs/GC electrode using the most cathodic deposition potential of -0.5 V which provided the highest average number of nanoparticles per square micrometer ($555 \pm 49\ \mu m^{-2}$) of very little average size (25 ± 12 nm) NPs. The simultaneous detection and quantification of O_2 and H_2O_2 was achieved only with electrodes functionalized using D-type Turkevich synthesis. In this case H_2O_2 was detected at the anode while current corresponding to O_2 reduction was selectively recorded at a potential close to -0.3 V without interference from H_2O_2.

1. Introduction

Both oxygen (O_2) and hydrogen peroxide (H_2O_2) are of outmost importance for living organisms and applications related to medical concern. O_2 is obviously essential for aerobic respiration of living cells [1]. It is also required for adenosine triphosphate (ATP) production in human cells, since it acts as final electron acceptor during oxidative phosphorylation reactions [2]. It has a key role in mitochondrial and normal tissue functions, but also in many common disease states, due to its dynamical regulation which maintains the balance between oxidative stress, hypoxia and anoxia [1]. Temporal variations in its local concentration may affect cell growth, differentiation, signaling, and free radical production [3]. O_2 deficiency results in a reduction in the energy levels that are required to maintain biological functions [2]. By its side, H_2O_2 is one of the most important reactive oxygen species (ROS), the role of which is ambivalent [4]. It is involved in the redox regulation of many biological processes, such as immune cell activation, vascular remodeling or apoptosis [5], and acts as intracellular messenger [6]. It is also a common intermediate or final byproduct in many enzyme-catalyzed biochemical reactions [7]. However, excess H_2O_2 in the organisms causes oxidative stress inside cells, resulting in damages to DNA, proteins, lipids and so on, thus leading to many pathologies over long periods, such as neurodegeneration, cardiovascular diseases, cancer and aging [5,8].

In this context, the detection and quantification of O_2 and H_2O_2 in physiological (i.e. neutral or nearly-neutral) conditions is actually of critical relevance. Since both O_2 and H_2O_2 exhibit redox activity, electrochemistry appears a method of choice to reach this goal, the main advantages of which, compared to other alternative methods, have been recently reviewed [4,9–11]. O_2 reduction reaction (ORR) has been extensively studied in both acidic and basic media with respect to energy storage concern [12], although studies in neutral media have gained interest with the rise of microbial fuel cells [13–16]. It is worth noting that many papers deal with mechanistic and kinetic aspects of ORR in neutral media rather than with O_2

* Corresponding author.
E-mail address: david.evrard@univ-tlse3.fr (D. Evrard).

https://doi.org/10.1016/j.ijoes.2023.100262
Received 19 September 2022; Accepted 14 October 2022
Available online 1 July 2023

detection. These latter aspects have been investigated on both bulk [17,18] and functionalized electrodes [19–24] by many authors including ourselves [18,21,22]. Moreover, O_2 monitoring in neutral media is often associated to environmental concerns such as water quality [25–27] or pesticides detection [28]. With respect to biological concern, several groups have reported on the in vivo measurement of O_2 content in brain cells [29–31]. By using a carbon fiber electrode coated by Nafion® and methylviologen, Mao et al. have put evidence for local O_2 changes in the brain of anesthetized rat before and during transient ischemia [29]. The amperometric response of the modified electrode was found linear in the range from 9 μM to 200 μM with a limit of detection (LOD) 5 μM. The group of Barbosa have used Pt microelectrode arrays which provided high resolution in vivo O_2 measurements in brain extracellular space [30,31]. In this latter case, a LOD down to 0.33 μM has been reported. The group of Schuhmann has even managed to visualize O_2 consumption of single living cells by using scanning electrochemical microscopy (SECM) with vibratory 10 μm Pt electrodes as SECM tips [32]. However, the commercially-available Clark-type sensor developed by Integra® LifeScience is often considered the gold standard for the intracranial measurement of local cerebral tissue O_2 levels [33]. With the aim of improving and miniaturizing such kind of invasive sensors, Luo et al. have proposed a flowing microfluidic platform for real-time monitoring of dissolved O_2 based on an Au paste working electrode [34]. However, this microfluidic device has not been tested in real biological environment.

H_2O_2 is much less studied than O_2, but in proportion there are more works dealing with its redox activity in neutral media. Contrary to what was observed for O_2, kinetics aspects are most of the time being ignored at the expense of detection, which can be achieved either in oxidation [35–37] or in reduction [38–43]. There are numerous examples of detection in biological environment. For instance, Nagarajan et al. have used an enzyme-functionalized GC electrode for H_2O_2 detection in ovarian cancer cell lines [44]. Other groups have also studied H_2O_2 release in mitochondria [45] and mouse macrophage cells [46]. Arbault's group has dedicated several works to H_2O_2 detection on black Pt-based electrodes, microelectrodes and microelectrodes array in biological living targets such as mitochondria or giant vesicles [47–49]. Using this material, a LOD down to 10 nM has been reported together with a linear range from a few to 40 μM H_2O_2 [47]. However, the question of simultaneous O_2 and H_2O_2 detection is rarely addressed although it is of outmost importance, since both species are related, H_2O_2 being a reduction product of O_2 and its own reduction occurring in the same potential range [50]. Amreen and Kumar have tested the possibility to detect O_2 and H_2O_2 using a single hematin-functionalized mesoporous carbon electrode, but calibration plots and subsequent detections have been carried out separately [51]. Arbault's group have also tried to detect both species using a single Pt-black microelectrode but their study has concluded that O_2 cannot be specifically measured on this latter material when H_2O_2 is present [49]. In order to fix this issue, Cheng et al. have developed an electrochemical multi-sensor device, in which O_2 and H_2O_2 detections have been achieved by different electrodes [52]. This system has allowed successful monitoring of O_2 consumption and H_2O_2 release in cardiac mitochondria. Urban et al. have also proposed a selective multianalyte detection method for in situ mapping of O_2 and H_2O_2 in microreactors [53].

In this work, we report on the kinetics study of H_2O_2 oxidation on bulk Au, GC and 6 different AuNPs-functionalized GC electrodes. AuNPs were prepared either by electrodeposition using constant potential electrolysis at different potential values or by chemical route, and further drop-casted onto GC surface in this latter case. The anodic transfer coefficient αn was calculated for all eight electrode materials using both Koutecky-Levich and Tafel treatment. The electrodes which afforded the best αn values were used for the simultaneous detection of O_2 and H_2O_2.

2. Experimental

2.1. Chemicals

$HAuCl_4$•3 H_2O (pro analysis grade) was purchased from Acros Organics. NaCl, $NaHCO_3$ and 30% H_2O_2 (analytical grade) were obtained from Fisher Scientific. $NaNO_3$ (suprapur grade) was supplied by Merck. Anhydrous trisodium citrate ($Na_3C_6H_5O_7$) and 98% sodium borohydride ($NaBH_4$) were purchased from Alfa Aesar. *N*-acetyl-L-cystein ($C_5H_9O_3NS$, NAC) (sigma grade) was purchased from Sigma Aldrich. 95% H_2SO_4 (normapur grade) was supplied by VWR Prolabo. 96% ethanol (ACS reagent) was from Fluka.

All the aqueous solutions were prepared using ultrapure water (Milli-Q, Millipore, 18.2 MΩ cm) and deaerated by bubbling Nitrogen during 10 min except for O_2 measurements. A gas stream was maintained over the solutions during experiments.

2.2. Apparatus

All the electrochemical experiments were carried out at controlled temperature in a standard three-electrode water-jacketed cell using a μ-Autolab II potentiostat (Metrohm) interfaced to a personal computer controlled with NOVA 1.9 software package (Metrohm). In the particular case of O_2 and H_2O_2 simultaneous detection, the experiments were performed by cyclic voltammetry using a Biologic VMP3 Multipotentiostat controlled by EC-Lab Express software. A Metrohm Ag/AgCl/KCl 3 M electrode, separated from the electrochemical cell by a Teflon PTFE capillary containing the support electrolyte solution and terminated by a ceramic diaphragm (D type), and a Metrohm glassy carbon (GC) wire were used as reference and counter electrodes, respectively. Working electrodes were GC (d = 3 mm, A = 7.069 mm^2) and Au (d = 2 mm, A = 3.142 mm^2) rotating disk electrodes from Radiometer.

2.3. Electrode preparation and functionalization

GC surfaces were polished successively by silicon carbide grinding paper (grit 1200) for 20 s, and by a 9 μm, 3 μm, 1 μm and 1/4 μm diamond powder (Presi) on a cloth polishing pad for 2 min. Au electrodes were polished successively by a silicon carbide grinding paper (grit 1200) for 10 s, and by 5 μm, 1 μm and 0.3 μm alumina slurry during 2 min. Between each polishing step, the electrodes were thoroughly rinsed with ultrapure water and then cleaned three times in an ultrasonic ethanol bath for 5 min. The electrode surface quality was finally checked by using a Nikon Eclipse LV150 optical microscope.

Electrodeposited gold nanoparticles (AuNPs) onto GC were prepared by constant potential electrolysis (CPE) at -0.5 V or 0.5 V for 1800 s in a deaerated 0.1 M $NaNO_3$ solution containing 0.25 mM $HAuCl_4$ (pH 3) as previously reported [21]. The corresponding deposits were depicted AuNPs(-0.5) and AuNPs(0.5).

Chemically-prepared AuNPs were synthesized according four different procedures. Synthesis A actually corresponds to the classical method described by Turkevich [54] and further refined by Frens [55]. Synthesis B was performed in a similar way to Synthesis A except that water was replaced by a 50/50 vol ratio H_2O/ethanol mixture. Synthesis C also corresponds to the Turkevich-Frens method, but *N*-acetyl-L-cystein (NAC) was also added after 20 min of reflux. In Synthesis D, $HAuCl_4$ was added to a sodium borohydride (3.4 ratio) aqueous solution under reflux. Immediately after this addition, an excess of NAC was added. All four syntheses were previously described in detail [22]. For the sake of clarity, the resulting AuNPs were depicted as AuNPs(X), X standing for A, B, C or D as a function of the corresponding synthesis. Electrode functionalization was achieved by drop-casting 50 μL of AuNPs(X) solution onto GC. After evaporation overnight, the AuNPs (X)/GC electrodes were dried in an oven for 1 h at 60 °C [22].

2.4. AuNPs-functionalized electrodes characterization

The AuNPs/GC surface was characterized by field emission gun scanning electron microscopy (FEG-SEM) at the CMEAB using a Quanta 250 FEG FEI equipment with an accelerating voltage of 5 kV and a working distance between 3 and 8 mm depending on the sample. Image analysis was carried out using a LGC homemade program for particles counting (density estimation) and average diameter measurement developed using MatLab image processing toolbox software.

2.5. Activation procedure

Prior to use, the functionalized electrodes were activated in a deaerated 0.5 M H_2SO_4 solution by running 30 scans between 0.2 V and 1.4 V at a scan rate of 100 mV s^{-1}, in accordance with the previously reported procedure [22].

3. Results and discussion

3.1. Kinetic study of H_2O_2 oxidation in neutral media

In order to gather basic data on H_2O_2 oxidation, this reaction was first investigated on unmodified GC and bare Au electrodes. Fig. 1 shows the steady-state voltammograms recorded on these latter materials in a deaerated NaCl/$NaHCO_3$ (0.15 M/0.028 M, pH 7.4) solution containing 0.24 mM H_2O_2. This medium was chosen in order to mimic human blood ionic composition [56].

On GC (red solid line), H_2O_2 oxidation appeared as an ill-defined wave the half-wave potential ($E_{1/2}$) of which was around 0.9 V, very close to the solvent discharge, thus condemning any exploitation of a current plateau. The corresponding oxidation reaction can be written as follow:

$$H_2O_2 \rightarrow O_2 + 2\,H^+ + 2\,e^-\ E^\circ = 0.695\ \text{V/SHE} \qquad \text{(R1)}$$

On Au (blue solid line), the voltammogram exhibited two oxidation peaks, located at 0.81 and 1.15 V, respectively. Since the voltammogram was recorded in a chloride-containing solution, the second peak, which was already observed in the blank (blue dashed line), may be associated to the formation of the $AuCl_4^-$ complex according to the following reaction [57,58]:

$$Au + 4\,Cl^- \rightarrow AuCl_4^- + 3\,e^-\ E^\circ = 1.002\ \text{V/SHE} \qquad \text{(R2)}$$

The first peak, which was not recorded when operating in the absence of H_2O_2, actually corresponds to its oxidation. This attribution is also supported by the corresponding peak potential value, which was very close to that of the $E_{1/2}$ observed on GC. The fact that this oxidation reaction leads to a peak despite the steady-state conditions may be accounted for considering the following spontaneous reaction which occurs between H_2O_2 and the $AuCl_4^-$ complex produced close to the electrode surface [59]:

$$2\,AuCl_4^- + 3\,H_2O_2 \rightarrow 2\,Au + 3\,O_2 + 6\,H^+ + 8\,Cl^- \qquad \text{(R3)}$$

This reaction induces a decrease in local H_2O_2 concentration close to the electrode surface, together with an increase in local Au amount, this latter leading to the increase in the second peak current observed between the blank and the curve recorded in the presence of H_2O_2.

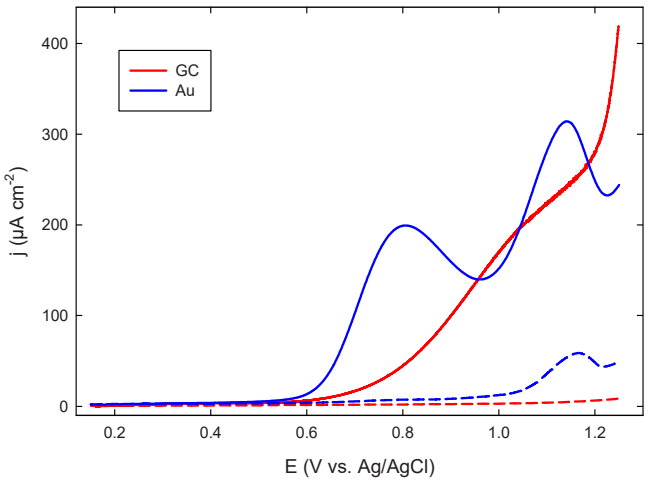

Fig. 1. Steady-state voltammograms recorded on GC (red) and Au (blue) electrodes in a deaerated NaCl/$NaHCO_3$ (0.15M/0.028 M, pH 7.4) solution containing (solid lines) or not (dashed lines) 0.24 mM H_2O_2. Scan rate: 1 mV s^{-1}; electrode rotation rate: 1400 rpm.

H_2O_2 oxidation was then examined on several AuNPs-functionalized GC electrodes. The AuNPs were prepared either by electrochemical methods or via chemical route. In this latter case, the colloidal suspension was drop-casted onto GC. The physicochemical features of the corresponding deposits are summarized in Table 1. With the aim of detecting simultaneously O_2 and H_2O_2, all these deposits were chosen because we have extensively investigated their reactivity toward O_2 reduction in previous works [21,22].

Fig. 2 shows the voltammograms obtained on these deposits in a deaerated NaCl/$NaHCO_3$ (0.15 M/0.028 M, pH 7.4) solution containing 0.24 mM H_2O_2. For the sake of clarity, the voltammograms of the blanks were not depicted. All six materials exhibited an anodic peak corresponding to H_2O_2 oxidation, in a similar way to what was observed on bulk Au (Fig. 1, blue solid line). However, depending on the AuNPs deposit, both the current and the potential associated to this peak were very different. AuNPs(0.5)/GC provided the response with the highest peak potential and the lowest peak current density, ca. 0.83 V and 30 μA cm^{-2}, respectively.

This deposit, which actually consisted in very few, big AuNPs was also the one that provided the worth response towards ORR amongst all electrochemically-prepared deposits [21]. Clearly, with a deposit of such low average density and large NP size, the advantages of the nanoarray of particles disappeared [60,61]. GC electrodes functionalized with AuNPs chemically prepared using Synthesis A, B and C afforded very similar responses with respect to H_2O_2 oxidation, Synthesis A providing the best response, with peak potentials in the range between 0.73 and 0.79 V and peak current densities from 75 to 120 μA cm^{-2}. Once again, these results compared favorably with those obtained for ORR study using the same deposits, AuNPs(A)/GC providing the best response, with 2 well-separated two-electron reduction processes located at -0.31 and -0.81 V [22]. A signal around twice higher was recorded on AuNPs(-0.5)/GC, with a peak current density ca. 210 μA cm^{-2}. This is consistent with our previous results showing that this latter deposits afforded a much higher response toward ORR than AuNPs (0.5)/GC [21]. Finally, the best response amongst all the tested deposits with respect to H_2O_2 oxidation was obtained on AuNPs(D)/GC, in terms of both peak potential (0.77 V) and peak current density (415 μA cm^{-2}). This such high current density value may be accounted for considering the high electroactive surface area afforded by the dense array of very small NPs which corresponds to AuNPs(D) deposit, as indicated in Table 1 [22].

In order to get further quantitative information upon H_2O_2 oxidation kinetics, steady-state voltammograms were recorded on all eight electrode materials at various rotation rates ω. Figs. 3A and 3B depicts the curves obtained for Au and bare GC electrodes, respectively, as an example. In both cases, the current density increased progressively with the increase in rotation rate, in accordance with a diffusion-limited electron transfer. The obtained data were treated using the well-known Koutecky-Levich equation [62,63]:

$$\frac{1}{j} = \frac{1}{j_k} + \frac{1}{j_d} = \frac{1}{n\ F\ k\ c} + \frac{1}{0.62\ n\ F\ D^{2/3}\ \omega^{1/2}\ \nu^{-1/6}\ c} \qquad (1)$$

Table 1
Average density and diameter of the different AuNPs deposits used.

AuNPs (X)	Electrodeposited		Chemically-prepared			
	-0.5 V	0.5 V	A	B	C	D
Average diameter (nm)	25 ± 12	315 ± 89	18 ± 4	10 ± 2	23 ± 6	2 ± 1
Average density (μm^{-2})	555 ± 49	9 ± 2	-[a]	-	-	318

[a] Because the deposits AuNPs(X) with X = A, B, C lacked of homogeneity, it was chosen not to provide any average density value, which would be meaningless.

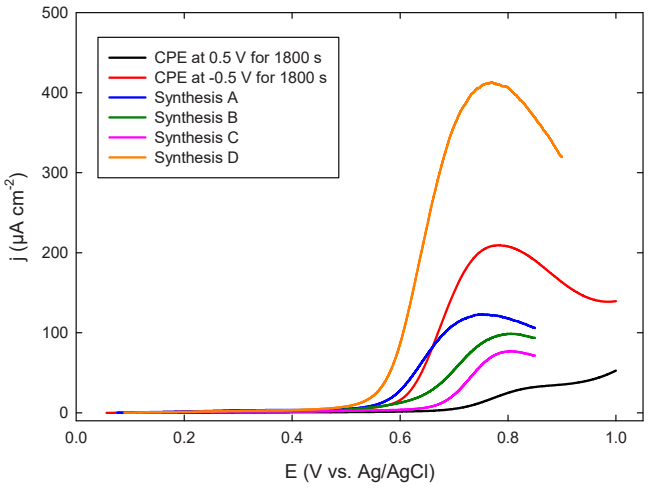

Fig. 2. Steady-state voltammograms recorded in a deaerated $NaCl/NaHCO_3$ (0.15 M/0.028 M, pH 7.4) solution containing 0.24 mM H_2O_2 on GC electrodes functionalized by AuNPs prepared using: (black) CPE at 0.5 V for 1800 s; (red) CPE at -0.5 V for 1800 s; (blue) Synthesis A; (green) Synthesis B; (pink) Synthesis C; (orange) Synthesis D. Scan rate: 1 mV s^{-1}; electrode rotation rate: 1400 rpm.

where j_k and j_d stand for the kinetic-limited and mass transfer-controlled current densities, respectively, F is the Faraday constant (96500 C mol^{-1}), k is the potential-dependent charge transfer rate constant, c is H_2O_2 bulk concentration (0.24 mM), D is H_2O_2 diffusion coefficient, and ν is the kinematic viscosity of the $NaCl/NaHCO_3$ (0.15 M/0.028 M, pH 7.4) aqueous solution.

Considering Eq. 1, the inverse of the current density 1/j was plotted as a function of the inverse of the square root of the rotation rate $1/\omega^{1/2}$ for several potential values ranging from 0.48 to 0.57 V for Au (Fig. 3C) and from 0.76 to 0.85 V for GC (Fig. 3D). For each potential value, a linear trend was found for the evolution of 1/j as a function of $1/\omega^{1/2}$. In each case, using the corresponding linear regression, the value of j_k was extracted from the intercept. Finally, the variation of Ln j_k was plotted as a function of the applied potential (Figs. 3E, 3F). The slope of the obtained linear regression plot allowed the anodic transfer coefficient αn to be calculated from the determination of the charge transfer constant k following Eq. (2):

$$k = k^{\circ}\, e^{\left(\frac{\alpha\, n\, F}{R\, T}\,(E - E^{\circ\prime})\right)} \quad (2)$$

where k° (cm s^{-1}) is the intrinsic charge transfer rate constant, R is the gas constant (8.31 J mol^{-1} K^{-1}), T is the temperature (298 K) and E°' is the apparent standard potential (V).

In order to strengthen our results, the αn determinations for all eight electrode materials were reproduced using the corrected Tafel treatment:

$$Ln\left(\frac{j \times j_{l,a}}{j_{l,a} - j}\right) = Ln\, j_0 + \frac{\alpha\, n\, F}{R\, T}\,(E - E^{\circ\prime}) \quad (3)$$

where $j_{l,a}$ stands for the anodic current density plateau and j_0 is the exchange current density. It is worth noting that, because of Reaction 3 which induces a peak rather than a plateau for H_2O_2 oxidation, the j_{peak} value was used for $j_{l,a}$ in the case of Au-based electrode materials.

The αn values obtained using both determination methods for Au, GC and the six AuNPs(X)/GC electrodes are summarized in Table 2.

Both Tafel and Koutecky-Levich treatments afforded αn values which compare favorably, showing the reliability of the data. As expected, the lowest αn values were obtained on unmodified materials (0.24 and 0.25 for Au and GC, respectively). Barely better values were found on AuNPs(B)/GC and AuNPs(C)/GC, in accordance with previous results on ORR [22]. AuNPs(X)/GC with X = 0.5, A and D allowed αn values around twice higher to be obtained. Once again, this result is consistent with our previous studies [21,22] although it is quite surprising to notice that AuNPs(0.5)/GC afforded a αn value so close to that found on AuNPs(A)/GC and AuNPs(D)/GC. Indeed, with respect to ORR, a βn value almost twice lower (ca. 0.29) was obtained using this latter electrode compared to the other two (0.59 and 0.55 for AuNPs (A)/GC and AuNPs(D)/GC, respectively). Finally, the best αn value was obtained on the AuNPs(-0.5)/GC electrode. As for ORR, this suggests that the best kinetics results are obtained using the most cathodic electrodeposition conditions. However, it is noteworthy that AuNPs (-0.5)/GC afforded such a high αn value compared to that found on AuNPs(A)/GC and AuNPs(D), since in the case of ORR all three electrodes gave rise to very similar βn values [21,22].

3.2. Simultaneous detection of O_2 and H_2O_2

The possibility to simultaneously detect O_2 and H_2O_2 was examined by using cyclic voltammetry on both AuNPs(-0.5)/GC and AuNPs(D)/GC. These latter electrodes were chosen as the ones that provided the best αn value amongst electrochemically and chemically prepared electrodes, respectively. Cyclic voltammetry was preferred to steady-state voltammetry in order to avoid any hydrodynamic perturbation of one rotating electrode by the other.

Fig. 4 A shows the cyclic voltammograms recorded simultaneously on two AuNPs(-0.5)/GC electrodes in an aerated $NaCl/NaHCO_3$ media in the absence and in the presence of H_2O_2. In the absence of H_2O_2 (black, dashed line), two reduction peaks were observed around -0.30 and -0.65 V which actually correspond to the two bielectronic reduction steps of O_2 [21]:

$$O_2 + 2\,H^+ + 2\,e^- \rightarrow H_2O_2\ E^{\circ} = 0.695\ V/SHE \quad (R4)$$

$$H_2O_2 + 2\,H^+ + 2\,e^- \rightarrow 2\,H_2O\ E^{\circ} = 1.776\ V/SHE \quad (R5)$$

On the anodic curve, no signal was noticed except the beginning of the oxidation peak of Au in the presence of Cl^- anions described by Reaction 2. When H_2O_2 was added to the solution, both anodic and cathodic curves changed of shape (red, solid line): on the former one, the oxidation peak of H_2O_2 appeared around 0.78 V; on the second one, both reduction peaks increased in current density. The fact that not only the second peak located at -0.65 V but also the first one at -0.30 V increased illustrates the interference of H_2O_2 on O_2 reduction, H_2O_2 reduction starting at a potential higher than -0.3 V, thus condemning any direct determination of this latter species. The evolution of the peak current densities upon addition of increasing amounts of H_2O_2 is depicted on Fig. 4B. As expected, the oxidation peak current density recorded at 0.78 V increased linearly upon H_2O_2 addition. Both reduction peak current densities also increased, in absolute terms, but surprisingly two slopes were observed. In both cases, the first slope corresponding to

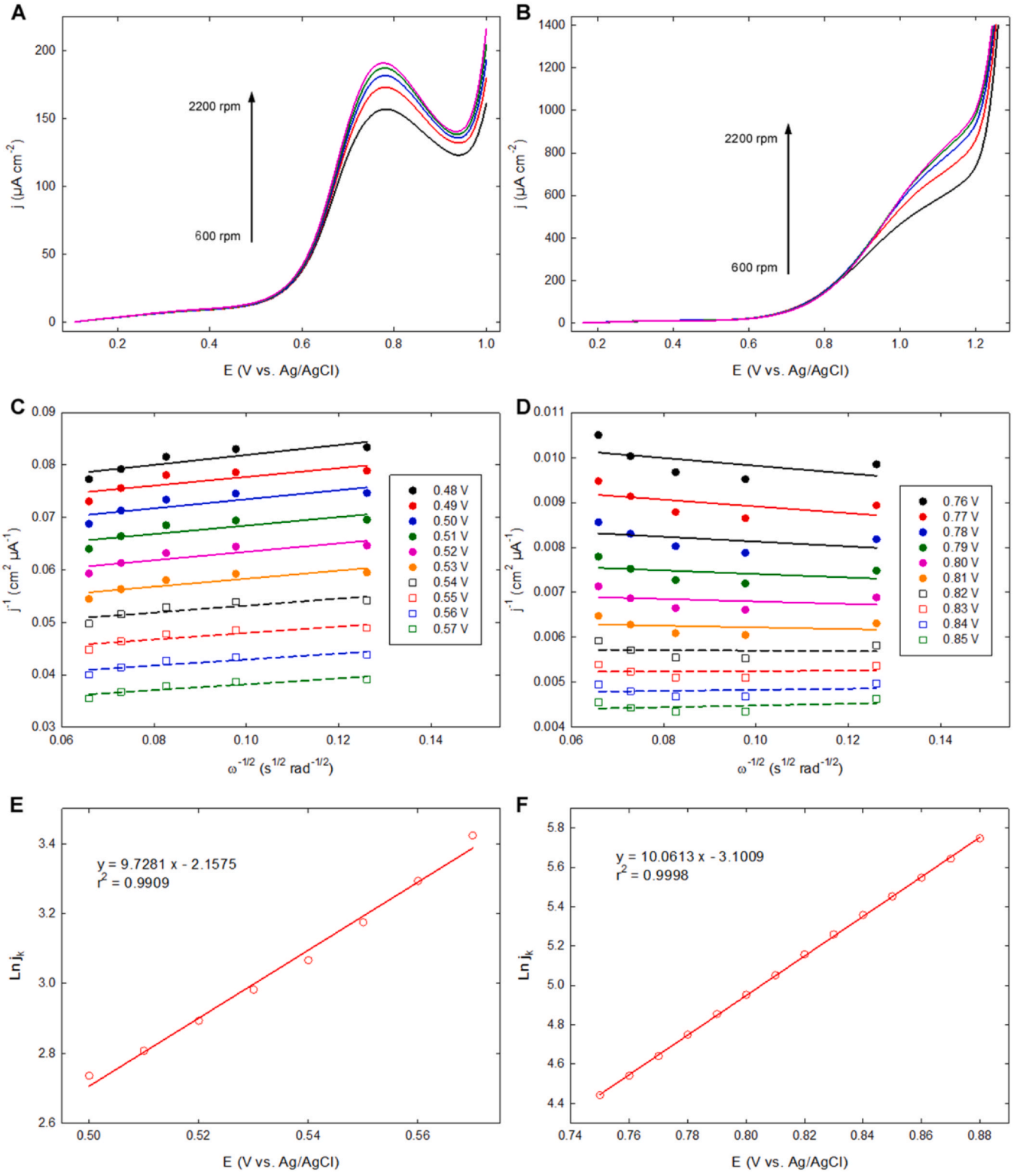

Fig. 3. Steady-state voltammograms recorded in a deaerated $NaCl/NaHCO_3$ (0.15 M/0.028 M, pH 7.4) solution containing 0.24 mM H_2O_2 using various rotation rate on (A) bulk Au and (B) bare GC electrodes; Corresponding Koutecky-Levich plots at different potentials (V vs. Ag/AgCl) on (C) bulk Au and (D) bare GC electrodes; Variation of the kinetic-limited current density Ln j_k corresponding to H_2O_2 oxidation as a function of the applied potential on (E) bulk Au and (F) bare GC electrodes.

the former additions of H_2O_2 was higher than the second one. This observation originates in a slight shift of the reduction peaks to more cathodic values which occurred all along the experiment, probably due to a progressive rearrangement of the AuNPs surface. In the case of the peak at -0.65, this problem could be easily overcome by changing the potential value where the current density is recorded for a more negative value. However, this would not be possible for the peak at -0.30 V, because of the presence of the second, more cathodic, reduction peak. It is also worth noting that the slopes corresponding to the peaks located at 0.78 and -0.65 V were different, although both peaks

Table 2
αn values corresponding to H_2O_2 oxidation on the different electrode materials investigated determined by Koutecky-Levich (KL) and Tafel treatment.

AuNPs (X)	Au	GC	-0.5	0.5	A	B	C	D
KL	0.21 ± 0.03	0.24 ± 0.04	0.61 ± 0.06	0.41 ± 0.07	0.59 ± 0.04	0.29 ± 0.09	0.28 ± 0.02	0.67 ± 0.04
Tafel	0.26 ± 0.03	0.26 ± 0.02	0.87 ± 0.02	0.64 ± 0.04	0.60 ± 0.01	0.35 ± 0.03	0.33 ± 0.05	0.63 ± 0.05
Average	0.24 ± 0.03	0.25 ± 0.03	0.78 ± 0.14	0.57 ± 0.14	0.60 ± 0.02	0.32 ± 0.04	0.31 ± 0.04	0.65 ± 0.05

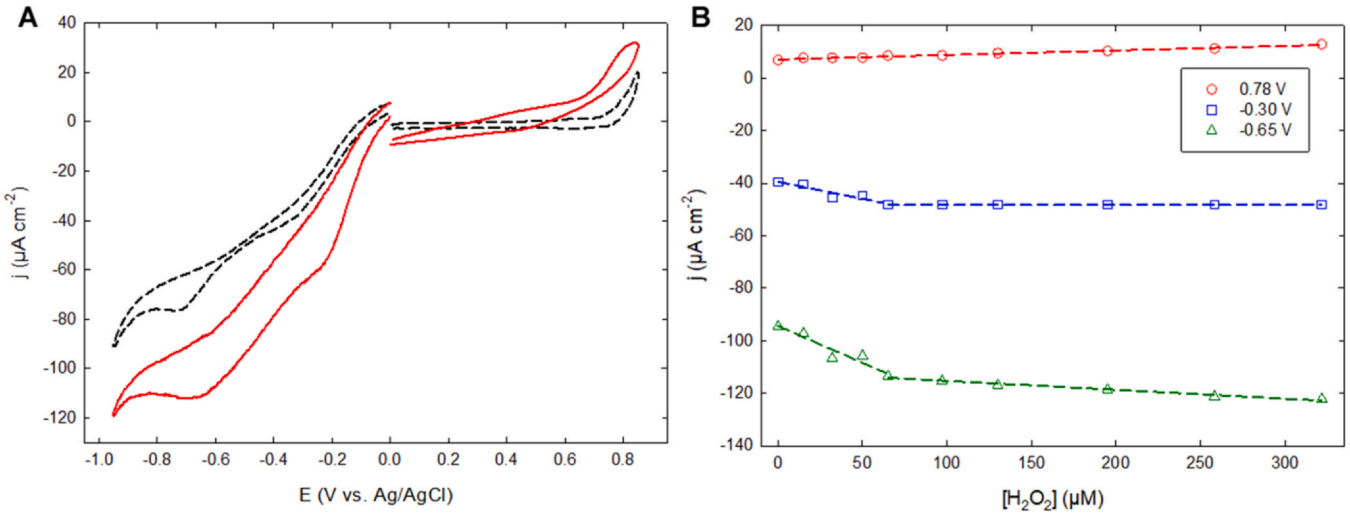

Fig. 4. (A) Cyclic voltammograms recorded simultaneously in oxidation and in reduction by means of a bipotentiostat in an aerated NaCl/$NaHCO_3$ (0.15 M/0.028 M, pH 7.4) solution containing (red, solid line) or not (black, dashed line) 0.24 mM H_2O_2 on two AuNPs(-0.5)/GC electrodes. Scan rate: 5 mV s^{-1}. (B) Evolution of the peak current density recorded at (red circle) 0.78 V; (blue square) -0.30 V; (green triangle) -0.65 V as a function of H_2O_2 concentration.

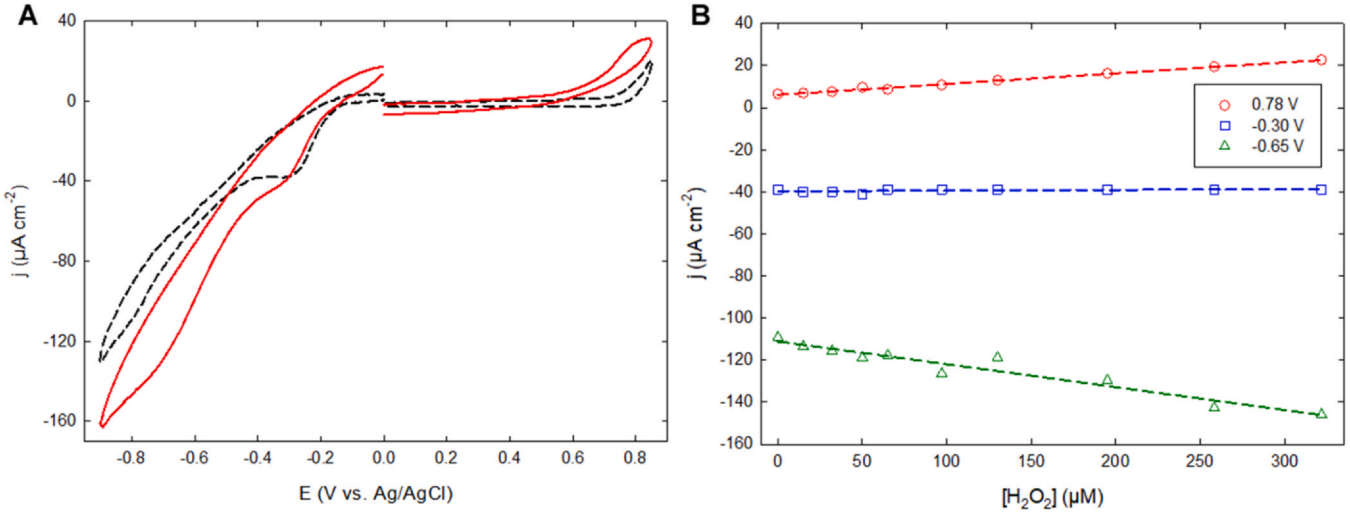

Fig. 5. (A) Cyclic voltammograms recorded simultaneously in oxidation and in reduction by means of a bipotentiostat in an aerated NaCl/$NaHCO_3$ (0.15 M/0.028 M, pH 7.4) solution containing (red, solid line) or not (black, dashed line) 0.24 mM H_2O_2 on two AuNPs(D)/GC electrodes. Scan rate: 5 mV s^{-1}. (B) Evolution of the peak current density recorded at (red circle) 0.78 V; (blue square) -0.30 V; (green triangle) -0.65 V as a function of H_2O_2 concentration.

are related to H_2O_2 redox activity. Indeed, the slope of the current density evolution for the oxidation peak was around twice smaller than that of the reduction peak. This can be accounted for considering Reaction 3, which induces a decrease in local H_2O_2 concentration close to the electrode surface during the oxidation process, thus leading to a smaller increase in peak current density. Similar cyclic voltammograms were obtained while operating using two AuNPs(D)/GC electrodes (Fig. 5 A): one oxidation peak was observed at 0.78 V together with two reduction peaks at -0.30 and -0.65 V, corresponding to Reactions 1, 4 and 5, respectively.

It is worth noting that in this case, the two steps of O_2 reduction were better separated than in the case of AuNPs(-0.5)/GC. Thus, AuNPs (D)/GC appears a better choice for simultaneous detection of O_2 and H_2O_2 than AuNPs(-0.5)/GC, despites it afforded lower αn and βn values. This was confirmed by the evolution of the peak current densities recorded at 0.78, -0.30 and -0.65 V upon addition of increasing amounts of H_2O_2 (Fig. 5B).

In this case, and contrary to what was observed on AuNPs(-0.5)/GC, the peak current density recorded at -0.30 V did not show any evolution when adding H_2O_2 up to 320 μM to the solution. The two peaks at 0.78 and -0.65 V increased linearly in current density with the increase in H_2O_2 concentration. In a similar way to what was observed on AuNPs (-0.5)/GC, the slope of the peak current density recorded at 0.78 V was smaller than that recorded at -0.65 V, once again because of Reaction 3.

It is noteworthy that on AuNPs(D)/GC a single slope was obtained for each signal evolution recorded, suggesting a good stability of this latter interface. Finally, this result demonstrates that it is possible to simultaneously detect and quantify O_2 and H_2O_2 by using a combination of the two calibration plots built by recording the current densities at 0.78 (for H_2O_2) and -0.30 (for O_2).

4. Conclusions

In this work, the kinetics of H_2O_2 oxidation in neutral media was studied on several unmodified and AuNPs-modified materials. Bulk Au and GC together with GC functionalized by AuNPs prepared either by electrodeposition or chemical route were tested. For each electrode material, αn values were determined by using both Koutecky-Levich and corrected Tafel treatment. Both methods afforded comparable values and showed that the best oxidation kinetics was obtained using the electrodes functionalized by the smallest chemically-prepared AuNPs (AuNPs(D)/GC) and the AuNPs electrodeposited using the lowest reduction potential (AuNPs(-0.5)/GC). These latter two electrodes were tested for O_2 and H_2O_2 simultaneous detection in a neutral $NaCl/NaHCO_3$ solution in order to mimic physiological conditions. The simultaneous detection appeared hardly possible on AuNPs(-0.5)/GC since the presence of H_2O_2 gave rise to a significant interference with respect to the signal corresponding to O_2 reduction. Moreover, a progressive rearrangement of the interface made the whole voltammetric response slightly shift to lower potential values all along the experiment. On the contrary, using AuNPs(D)/GC electrodes, O_2 reduction peak was free from any interference from H_2O_2 and the interface response proved remarkably stable with time. Thus, using this latter material, the simultaneous electrochemical detection of O_2 and H_2O_2 is actually possible. This result is promising for simultaneous amperometric quantification of O_2 and H_2O_2 in physiological conditions and even in biological tissues. Tests in real samples are currently running and will be reported in due course.

Declaration of Competing Interest

The authors declare that they have no known competing financial interests or personal relationships that could have appeared to influence the work reported in this paper.

References

[1] D.B. Papkovsky, R.I. Dmitriev, Imaging of oxygen and hypoxia in cell and tissue samples, Cell. Mol. Life Sci. 75 (2018) 2963–2980.
[2] K. Hirota, Basic biology of hypoxic responses mediated by the transcription factor HIFs and its implication for medicine, Biomedicines 8 (2020) 32.
[3] T.L. Place, F.E. Domann, A.J. Case, Limitations of oxygen delivery to cells in culture: an underappreciated problem in basic and translational research, Free Radic. Biol. Med 113 (2017) 311–322.
[4] S. Zhao, G. Zang, Y. Zhang, H. Liu, N. Wang, S. Cai, C. Durkan, G. Xie, G. Wang, Recent advances of electrochemical sensors for detecting and monitoring ROS/RNS, Biosens. Bioelectron. 179 (2021) 113052.
[5] H. Yang, L. Yuan, J. Liu, X. Dong, Study on detection methods for H2O2 in biological samples, Int. J. Chem. Stud. 4 (2016) 18–21.
[6] S.G. Rhee, Redox signaling: Hydrogen peroxide as intracellular messenger, Exp. Mol. Med. 31 (1999) 53–59.
[7] W. Chen, S. Cai, Q.-Q. Ren, W. Wen, Y.-D. Zhao, Recent advances in electrochemical sensing for hydrogen peroxide: a review, Analyst 137 (2012) 49–58.
[8] Y. Zhang, K. Hu, Z. Ling, W. Di, A. MnO_2, $Ru(dpp)_3]Cl_2$ system for colorimetric and fluorimetric dual-readout detection of H2O2, RSC Adv. 9 (2019) 7803–7810.
[9] S. Borgmann, Electrochemical quantification of reactive oxygen and nitrogen: challenges and opportunities, Anal. Bioanal. Chem. 394 (2009) 95–105.
[10] C. Calas-Blanchard, G. Catanante, T. Noguer, Electrochemical sensor and biosensor strategies for ROS/RNS detection in biological systems, Electroanalysis 26 (2014) 1277–1286.
[11] M. Malferrari, M. Becconi, S. Rapino, Electrochemical monitoring of reactive oxygen/nitrogen species and redox balance in living cells, Anal. Bioanal. Chem. 411 (2019) 4365–4374.
[12] C. Song, J. Zhang, Electrocatalytic oxygen reduction reaction, PEM fuel cell electrocatalysts and catalyst layers, Springer, London, 2008.
[13] J. Wu, Y. Wang, D. Zhang, B. Hou, Studies on the electrochemical reduction of oxygen catalyzed by reduced graphene sheets in neutral media, J. Power Sources 196 (2011) 1141–1144.
[14] Y. Lu, N. Zhu, F. Yin, T. Yang, P. Wu, Z. Danga, M. Liu, X. Weia, Biomass-derived heteroatoms-doped mesoporous carbon for efficient oxygen reduction in microbial fuel cells, Biosens. Bioelectron. 98 (2017) 350–356.
[15] N. Zhu, Y. Lu, B. Liu, T. Zhang, J. Huang, C. Shi, P. Wu, Z. Dang, R. Wang, CoMn2O4-supported functionalized carbon nanotube: efficient catalyst for oxygen reduction in microbial fuel cells, J. Nanopart. Res 19 (2017) 1–11.
[16] Y. Liu, Z.M. Liu, Promoted activity of nitrogen-doped activated carbon as a highly efficient oxygen reduction catalyst in microbial fuel cells, J. Appl. Electrochem 49 (2019) 119–133.
[17] M.S. El-Deab, T. Okajima, T. Ohsaka, Electrochemical reduction of oxygen on gold nanoparticle-electrodeposited glassy carbon electrodes, J. Electrochem. Soc. 150 (2003) A851–A857.
[18] G. Gotti, K. Fajerwerg, D. Evrard, P. Gros, Kinetics of dioxygen reduction on gold and glassy carbon electrodes in neutral media, Int. J. Electrochem. Sci. 8 (2013) 12643–12657.
[19] C.R. Raj, A.I. Abdelrahman, T. Ohsaka, Gold nanoparticle-assisted electroreduction of oxygen, Electrochem. Commun. 7 (2005) 888–893.
[20] J.H. Shim, J. Kim, C. Lee, Y. Lee, Electrocatalytic activity of gold and gold nanoparticles improved by electrochemical pretreatment, J. Phys. Chem. C. 115 (2011) 305–309.
[21] G. Gotti, K. Fajerwerg, D. Evrard, P. Gros, Electrodeposited gold nanoparticles on glassy carbon: correlation between nanoparticles characteristics and oxygen reduction kinetics in neutral media, Electrochim. Acta 128 (2014) 412–419.
[22] G. Gotti, D. Evrard, K. Fajerwerg, P. Gros, Oxygen reduction reaction features in neutral media on glassy carbon electrode functionalized by chemically prepared gold nanoparticles, J. Solid State Electrochem 20 (2016) 1539–1550.
[23] S. Zhang, O. Oms, L. Hao, R. Liu, M. Wang, Y. Zhang, H.-Y. He, A. Dolbecq, J. Marrot, B. Keita, L. Zhi, P. Mialane, B. Li, G. Zhang, High oxygen reduction reaction performances of cathode materials combining polyoxometalates, coordination complexes, and carbonaceous supports, ACS Appl. Mater. Interfaces 9 (2017) 38486–38498.
[24] J.-W. Chen, Z. Zhang, H.-M. Yan, G.-J. Xia, H. Cao, Y.-G. Wang, Pseudo-adsorption and long-range redox coupling during oxygen reduction reaction on single atom electrocatalyst, Nat. Commun. 13 (2022) 1734.
[25] A. Rahim, L.S.S. Santos, S.B.A. Barros, L.T. Kubota, Y. Gushikem, Dissolved O2 sensor based on cobalt(II) phthalocyanine immobilized in situ on electrically conducting carbon ceramic mesoporous SiO_2/C material, Sens. Actuators, B 177 (2013) 231–238.
[26] D.-H. Zhao, S. Palanisamy, S.-M. Chen, Electrochemical detection of dissolved oxygen in water using a composite of graphene oxide and platinum nanoparticles, Int. J. Electrochem. Sci. 10 (2015) 10038–10044.
[27] K.S. Shalini Devi, A. Jain, S.-T. Huang, A. Senthil, Kumar, Metal and heteroatoms-free carbon soot obtained from atmospheric combustion of naphthalene for sensitive dissolved oxygen reduction reaction and sensing in neutral media, Electrochim. Acta 296 (2019) 407–417.
[28] X. Luo, Z. Luo, X. Wei, L. Jiao, Q. Fang, H. Wang, J. Wang, W. Gu, L. Hu, C. Zhu, Iridium single-atomic site catalysts with superior oxygen reduction reaction activity for sensitive monitoring of organophosphorus pesticides, Anal. Chem. 94 (2021) 1390–1396.
[29] L. Mao, J. Jin, L.-n Song, K. Yamamoto, L. Jin, Electrochemical microsensor for in vivo measurements of oxygen based on Nafion and methylviologen modified carbon fiber microelectrode, Electroanalysis 11 (1999) 499–504.
[30] A. Ledo, C.F. Lourenço, J. Laranjinha, C.M.A. Brett, G.A. Gerhardt, R.M. Barbosa, Ceramic-based multisite Pt microelectrode arrays: Morphological characteristics and electrochemical performance in brain tissue, Inorg. Chem. 89 (2017) 1674–1683.
[31] A. Ledo, E. Fernandes, J.E. Quintero, G.A. Gerhardt, R.M. Barbosa, Electrochemical evaluation of a multi-site clinical depth recording electrode for monitoring cerebral tissue Oxygen, Micromachines 11 (2020) 632.
[32] M. Nebel, S. Grützke, N. Diab, A. Schultec, W. Schuhmann, Microelectrochemical visualization of oxygen consumption of single living cells, Faraday Discuss. 164 (2013) 19–32.
[33] G. Huschak, T. Hoell, C. Hohaus, C. Kern, Y. Minkus, H.-J. Meisel, Clinical evaluation of a new multiparameter neuromonitoring device. Measurement of brain tissue Oxygen, brain temperature, and intracranial pressure, J. Neurosurg. Anesth. 21 (2009) 155–160.
[34] J. Luo, T. Dziubla, R. Eitel, A low temperature co-fired ceramic based microfluidic Clark-typeoxygen sensor for real-time oxygen sensing, Sens. Actuators, B 240 (2017) 392–397.
[35] A.M. Oliveira Brett, F.-M. Matysik, M.T. Vieira, Thin-film gold electrodes produced by magnetron sputtering. Voltammetric characteristics and application in batch injection analysis with amperometric detection, Electroanalysis 9 (1997) 209–212.
[36] M. Gerlache, Z. Senturk, G. Quarin, J.-M. Kauffmann, Electrochemical behavior of H_2O_2 on gold, Electroanalysis 9 (1997) 1088–1092.
[37] M. Gerlache, S. Girousi, G. Quarin, J.-M. Kaffmann, Pulsed electrochemical detection of H_2O_2 on gold, Electrochim. Acta 43 (1998) 3467–3473.
[38] S. Wu, J. Liu, X. Bai, W. Tan, Stability improvement of Prussian blue by a protective cellulose acetate membrane for hydrogen peroxide sensing in neutral media, Electroanalysis 22 (2010) 1906–1910.
[39] P. Salazar, M. Martín, R.D. O'Neill, R. Roche, J.L. González-Mora, Improvement and characterization of surfactant-modified Prussian blue screen-printed carbon electrodes for selective H_2O_2 detection at low applied potentials, J. Electroanal. Chem. 674 (2012) 48–56.
[40] C. Gaviglio, F. Battaglini, Hydrogen peroxide detection under physiological conditions by Prussian blue stabilized using a polyelectrolyte-surfactant complex matrix, Sens. Actuators, B 182 (2013) 53–57.

[41] F. Doroftei, T. Pinteala, A. Arvinte, Enhanced stability of a Prussian blue/sol-gel composite for electrochemical determination of hydrogen peroxide, Microchim. Acta 181 (2014) 111–120.
[42] Z. Wang, F. Xie, Z. Liu, G. Du, A.M. Asiri, X. Sun, High-performance non-enzyme hydrogen peroxide detection in neutral solution: Using a Nickel borate nanoarray as a 3D electrochemical sensor, Chem. Eur. J. 23 (2017) 16179–16183.
[43] S.C. Silva, R.M. Cardoso, E.M. Richter, R.A.A. Munoz, E. Nossol, Reduced graphene oxide/multi-walled carbon nanotubes/prussian blue nanocomposites for amperometric detection of strong oxidants, Mater. Chem. Phys. 250 (2020) 123011.
[44] R.D. Nagarajan, P. Murugan, K. Palaniyandi, R. Atchudan, A.K. Sundramoorthy, Biocompatible MXene ($Ti_3C_2T_x$) immobilized with flavin adenine dinucleotide as an electrochemical transducer for hydrogen peroxide detection in ovarian cancer cell lines, Micromachines 12 (2021) 862.
[45] S. Rapino, R. Marcu, F. Paolucci, M. Giorgio, Electrochemical detection of H_2O_2 formation in isolated mitochondria, Methods Enzym. 526 (2013) 123–134.
[46] P. Balasubramanian, M. Annalakshmi, S.-M. Chen, T. Sathesh, T.-K. Peng, T.S.T. Balamurugan, Facile solvothermal preparation of Mn2CuO4 microspheres: Excellent electrocatalyst for real-time detection of H_2O_2 released from live cells, ACS Appl. Mater. Interfaces 10 (2018) 43543–43551.
[47] S. Ben-Amor, E. Vanhove, F.S. Belaïdi, S. Charlot, D. Colin, M. Rigoulet, A. Devin, N. Sojic, J. Launay, P. Temple-Boyer, S. Arbault, Enhanced detection of hydrogen peroxide with platinized microelectrode arrays for analyses of mitochondria activities, Electrochim. Acta 126 (2014) 171–178.
[48] V. Badet, J. Pandard, N. Sojic, S. Arbault, Deciphering the platinized surface reactivity to improve the detection of hydrogen peroxide in bioanalyses, ChemElectroChem 3 (2016) 2288–2296.
[49] P. Lefrançois, Jm Santolini, S. Arbault, Electroanalysis at a single giant vesicle generating enzymatically a reactive oxygen species, Anal. Chem. 93 (2021) 13143–13151.
[50] C.C.M. Neumann, E. Laborda, K. Tschulik, K.R. Ward, R.G. Compton, Performance of silver nanoparticles in the catalysis of the oxygen reduction reaction in neutral media: Efficiency limitation due to hydrogen peroxide escape, Nano Res. 6 (2013) 511–524.
[51] K. Amreen, A.S. Kumar, Highly redox-active hematin-functionalized Carbon mesoporous nanomaterial for electrocatalytic reduction applications in neutral media, ACS Appl. Nano Mater. 1 (2018) 2272–2283.
[52] M.-H. Cheng, A.J. Chicco, D. Ball, T.W. Chen, Analysis of mitochondrial oxygen consumption and hydrogen peroxide release from cardiac mitochondria using electrochemical multi-sensors, Sens. Actuators, B 360 (2022) 131641.
[53] S. Urban, B.J. Deschner, L.L. Trinkies, J. Kieninger, M. Kraut, R. Dittmeyer, G.A. Urban, A. Weltin, In situ mapping of H2, O2, and H2O2 in microreactors: a parallel, selective multianalyte detection method, ACS Sens. 6 (2021) 1583–1594.
[54] J. Turkevich, P.C. Stevenson, J. Hillier, A study of the nucleation and growth processes in the synthesis of colloidal gold, Discuss. Faraday Soc. 11 (1951) 55–75.
[55] G. Frens, Controlled nucleation for the regulation of the particle size in monodisperse gold suspensions, Nat. Phys. Sci. 241 (1973) 20–22.
[56] E.B. Hendry, The osmotic pressure and chemical composition of human body fluids, Hum. Body Fluids 8 (1962) 246–265.
[57] A. Ringbom, Complexation in Analytical Chemistry, John Wiley & Sons Inc, New York, 1963.
[58] T. Hezard, L. Laffont, P. Gros, P. Behra, D. Evrard, Hg(II) trace electrochemical detection on gold electrode: Evidence for chloride adsorption as the responsible for the broad baseline, J. Electroanal. Chem. 697 (2013) 28–31.
[59] S. Bourigua, A. Maaref, F. Bessueille, N. Jaffrezic, Renault, A new design of electrochemical and optical biosensors based on biocatalytic growth of Au nanoparticles – example of glucose detection, Electroanalysis 25 (2013) 644–651.
[60] T. Hezard, K. Fajerwerg, D. Evrard, V. Colliere, P. Behra, P. Gros, Influence of the gold nanoparticles electrodeposition method on Hg(II) trace electrochemical detection, Electrochim. Acta 73 (2012) 15–22.
[61] T. Hezard, K. Fajerwerg, D. Evrard, V. Colliere, P. Behra, P. Gros, Gold nanoparticles electrodeposited on glassy carbon using cyclic voltammetry: application to Hg(II) trace determination, J. Electroanal. Chem. 664 (2012) 46–52.
[62] J. Koutecky, Kinetics of electrode processes. XI. The polarographic current due to an electrode process preceded by a chemical reaction in solution between reactants differing in their diffusion coefficients, Chem. Listy Vedu Prum 47 (1953) 1758–1761.
[63] S. Treimer, A. Tanga, D.C. Johnson, A consideration of the application of Koutecky-Levich plots in the diagnoses of charge-transfer mechanisms at rotated disk electrodes, Electroanalysis 14 (2002) 165–171.